

Non-perturbative dynamics of correlated disordered flat-band system

Qi Li,^{1,2} Junfeng Liu,³ Zi-Xiang Hu,⁴ and Zhou Li^{1,2,5,*}

¹*GBA Branch of Aerospace Information Research Institute,
Chinese Academy of Sciences, Guangzhou 510535, China*

²*Guangdong Provincial Key Laboratory of Terahertz Quantum Electromagnetics, Guangzhou 510700, China*

³*School of Physics and Materials Science, Guangzhou University, Guangzhou 510006, China*

⁴*Department of Physics and Chongqing Key Laboratory for Strongly Coupled Physics,
Chongqing University, Chongqing 401331, China*

⁵*University of Chinese Academy of Sciences, Beijing 100039, China*

(Dated: May 31, 2023)

We develop a numerical method for the time evolution of Gaussian wave packet on a flat-band lattice in the presence of correlated disorder. We apply this to the one-dimensional (1D) cross-stitch model. Reasonable agreements with analytical results from the quantum master equation are found, for the decay and dephasing process when the flat-band intersects with the dispersive band. Extending the numerical method to the two dimensional (2D) $\alpha - T_3$ model, we find the initial flat-band wave packet preserves its localization when $\alpha = 0$ regardless of disorders and intersections; and it shifts in real space when $\alpha \neq 0$. We point out a method to generate random on-site energy with a prescribed correlation, derive the imaginary error function and the coupled equations of the flat-band and dispersive-band in 1D.

Introduction.—Flat-band systems possess completely dispersionless single-particle energy states of which the effective mass diverges. Flat-bands were introduced as early as 1989, when Lieb proved two theorems on the Hubbard model [1], discovering flat-band ferrimagnetism[2] in the repulsive Hubbard model comprised of a bipartite lattice, with the number of sites in the sub-lattices unequal. Flat-bands have also been found in certain decorated lattices [3, 4] with single electron compact localized states, and more recently in sawtooth lattices with compactification tuning for nonlinear localized modes [5].

A nearly flat band is found in the Holstein model [6] near the adiabatic limit. The effective mass is very large but does not diverge, so the quasiparticle is described by the Fermi liquid not the Luttinger liquid theory. Topological flat-bands with non-zero Chern number is realized in certain short-range tight binding models and is helpful to understand the fractional quantum Hall effect[7, 8]. Remarkably, a two-dimension (2D) lattice model called the $\alpha - T_3$ model interpolates between the well-known graphene honeycomb lattice ($\alpha = 0$) and the dice lattice ($\alpha = 1$). The latter is realized in a tri-layer structure of cubic lattices along the (111) direction (e.g. SrTiO₃/SrIrO₃/SrTiO₃ [9]). Moreover, the intermediate $\alpha = 1/\sqrt{3}$ is achieved at a critical doping of Hg_{1-x}Cd_xTe with intriguing orbital magnetic response[10]. The Berry phase [11] is continuously tuned from π to 0 as α changes from 0 to 1, while the energy band-structure is unchanged. In topological insulators with particle hole asymmetry[12], Berry phase is 0 in the non-relativistic Schrodinger regime and π in the relativistic Dirac regime, the two regimes could not be connected in a continuous way. The $\alpha - T_3$ model connects them without a Schrodinger term. Recently, flat-band is re-

alized in many twisted bi-layer structures such as boron nitride, graphene and indium selenide [13–15]. The integration of high quality twisted bi-layer flat-band material in a wave-guide or cavity, to make optoelectronic prototype devices, is promising.

In the area of photonic topological insulators (e.g. photonic Floquet topological insulators [16]), which was motivated by Haldane’s paper to design directional optical waveguides in photonic crystals [17], flat edge states emerge as a consequence of topology. Due to the recent progress in experimental expertise, flat-bands can now be created, e.g., by tailoring the exciton-polaritons in arbitrary lattices [18], or in arrays of evanescently coupled optical waveguides [19, 20]. Recently in quasi one-dimensional (1D) photonic system, flatband is generated in the experiment of the photonic Aharonov–Bohm cage. Correlated disorder is added in the experiment and the inverse Anderson localization is observed [21–25].

In this work, we study the time evolution of flat-band states in 1D and 2D systems in the presence of correlated disorders. Such disorders usually appear in photons not in materials. The set-up of correlated disorders in flat-band materials brings interesting Gaussian wave packet dynamics. In 1D cross-stitch model, we are able to tune the decay and dephasing by setting correlated or anti-correlated disorders. In 2D $\alpha - T_3$ model, we observe the wave packet shifts from its original position in real space when $\alpha \neq 0$.

1D model.—Flat-band appears in the cross-stitch lattice model, as shown in the Fig. 1(a). All neighboring

sites are connected, and the Hamiltonian is written as

$$\begin{aligned} \hat{H}_0 = & -t_{ab} \sum_j (|a_j\rangle\langle b_j| + |b_j\rangle\langle a_j|) \\ & - J \sum_{j,\delta} (|a_j\rangle\langle a_{j+\delta}| + |a_j\rangle\langle b_{j+\delta}| + |b_j\rangle\langle b_{j+\delta}| + |b_j\rangle\langle a_{j+\delta}|), \end{aligned} \quad (1)$$

where $|a_j\rangle$ and $|b_j\rangle$ are two parallel sub-lattices, j is an integer number and $\delta = \pm 1$ is used to denote the nearest neighbour sites in one dimension. In the absence of the on-site potential, there are exactly one flat-band $E_f = t_{ab}$ and one dispersive band $E_d(p) = -4J \cos(p) - t_{ab}$, with p the momentum. The lattice constant and the Planck constant \hbar are set to be 1. The intersections of the two bands are given by $p_{1,2} = \pm \arccos(-t_{ab}/2J)$. In order to have intersections, $|-t_{ab}/2J| \leq 1$ must be satisfied. Here t_{ab} is the intra-cell hopping. Tuning t_{ab} changes the positions of the two bands while keeping the shapes unchanged, as shown in the Fig. 1(b).

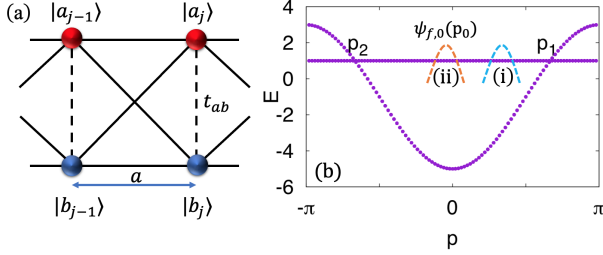


FIG. 1. (Color online) The cross-stitch lattice structure. (a) Each unit cell $|j\rangle$ contains two parallel sites $|a_j\rangle$ and $|b_j\rangle$. t_{ab} is the intra-cell hopping strength. (b) The model contains two bands, one flat-band and one dispersive band with intersections at $p_{1,2}$ in momentum space. A Gaussian wave packet initially propagates in the flat-band with different initial average momentums.

Correlated disorders.—Random onsite disorder potentials in the cross-stitch model modify the onsite energy $V_\epsilon^{a,b}(j)$, where ϵ denotes different disorder realizations. For simplicity, the disorder potential vanishes on average with $\hat{H} = \hat{H}_0$, and for each disorder realization we define the intra- and inter-sub-lattice disorder correlations. Explicitly the intra-sublattice correlations are assumed to be the same for $|a_j\rangle$ and $|b_j\rangle$ sublattices such that $G_{aa}(q) = G_{bb}(q) \equiv G_0(q)$. The inter-sublattice correlations are assumed to have the same form as the intra-sublattice correlations but only differ by a pre-factor δ_{ab} so $C_{ab}(q) = C_{ba}(q) \equiv G_1(q) = \delta_{ab}C_0(q)$. Here $\delta_{ab} = 0, +1, -1$ correspond to uncorrelated, fully correlated and fully anti-correlated sub-lattice potentials, respectively. For Gaussian type of correlations considered here, $C_{\sigma\sigma}(x) = C_0 e^{-(x/\ell)^2}$, we have $G_0(q) = \frac{C_0 \ell}{2\sqrt{\pi} \hbar} \exp[-\frac{1}{4}(\frac{q\ell}{\hbar})^2]$.

To generate the random on-site energy $V_\epsilon^{a,b}(x)$ from

a prescribed correlation function $G_0(q)$, we use the convolution method [26]. The modulation function $M(x)$, which is the Fourier transform of $[G_0(q)]^{1/2}$, is given by

$$M(x) = \int_{-\infty}^{\infty} [G_0(q)]^{\frac{1}{2}} e^{iqx} dq = 2\sqrt{C_0 \sqrt{\pi} / \ell} e^{-2(x/\ell)^2}. \quad (2)$$

The convolution of the delta-correlated random number $\alpha(x)$ with the modulation function gives the correlated $V_\epsilon^{a,b}(x)$ in real space:

$$V_\epsilon^{a,b}(x) = \int_{-\infty}^{\infty} dx' \alpha(x-x') M(x') \quad (3)$$

with $\alpha(x)$ satisfying the standard properties $\langle \alpha(x) \rangle = 0$ and $\langle \alpha(x)\alpha(x') \rangle = \delta(x-x')$.

Master equation—At short times, the quantum master equation accurately describes the ensemble averaged dynamics of disordered models and the incoherent nature mainly emerges in the second-order term, i.e., the Lindblad term [27–29].

$$\begin{aligned} \partial_t \bar{\rho}(t) = & -\frac{i}{\hbar} [\hat{H}_{eff}, \bar{\rho}(t)] + \sum_{\alpha \in \{\pm 1\}} \frac{2\alpha}{\hbar^2} \int_{-\infty}^{\infty} dq \\ & \times \sum_{\beta \in \{-1, 0, 1\}} \tilde{G}_\beta(q) \int_0^t dt' \mathcal{L}(\hat{L}_{q,\beta}^{(\alpha)}(t'), \bar{\rho}(t)) \end{aligned} \quad (4)$$

where $\mathcal{L}(\hat{L}, \rho) = \hat{L}\rho\hat{L}^\dagger - \frac{1}{2}\hat{L}^\dagger\hat{L}\rho - \frac{1}{2}\rho\hat{L}^\dagger\hat{L}$ and $\tilde{G}_0(q) = G_0(q)(1 + \delta_{ab})/2$, $\tilde{G}_1(q) = \tilde{G}_{-1}(q) = G_0(q)(1 - \delta_{ab})/4$. The effective Hamiltonian $\hat{H}_{eff}(t)$ and the Lindblad operators $\hat{L}_{q,\beta}^{(\alpha)}(t)$ (for details see [30]). Introducing transformations $|d\rangle = (|a\rangle + |b\rangle)/\sqrt{2}$ and $|f\rangle = (|a\rangle - |b\rangle)/\sqrt{2}$ [31, 32], the disorder potential is rewritten as $\hat{V}_\epsilon = V_\epsilon^+(\hat{x}) \otimes (|f\rangle\langle f| + |d\rangle\langle d|) + V_\epsilon^-(\hat{x}) \otimes \hat{\sigma}_x$, with $V_\epsilon^\pm(\hat{x}) = \frac{1}{2}(V_\epsilon^a(\hat{x}) \pm V_\epsilon^b(\hat{x}))$ and $\hat{\sigma}_x = |f\rangle\langle d| + |d\rangle\langle f|$. Clearly, $V_\epsilon^-(\hat{x})$ indicate the inter-band coupling between the flat band $|f\rangle$ and the dispersive band $|d\rangle$. It vanishes when $V_\epsilon^a(\hat{x}) = V_\epsilon^b(\hat{x})$, i.e., the $\delta_{ab} = 1$ case.

It's reasonable to treat the dispersive band linearly in the vicinities of the intersections which dominates the decay of flat-band states:

$$\hat{H} = v(\hat{p} - p_1) \otimes |d\rangle\langle d| \quad (5)$$

where velocity v is the dispersive band slope at the intersections and we assume the flat-band states extends over a few lattice unit cells (continuum limit). Under linear approximation, projecting $\bar{\rho}$ on to flat and disper-

sive bands in momentum space respectively, we obtain:

$$\begin{aligned}
& \partial_t \bar{\rho}_f(p) \\
&= \frac{2t}{\hbar^2} \int_{-\infty}^{\infty} dq \tilde{G}_0(q) \{ \bar{\rho}_f(p-q) - \bar{\rho}_f(p) \} \\
&\quad - \sum_{j=1,2} \Gamma_t^{(j)}(p_j - p) \bar{\rho}_f(p) \\
&\quad + \sum_{j=1,2} \frac{4t}{\hbar^2} \int_{-\infty}^{\infty} dq \tilde{G}_1(q) \text{sinc}\left[\frac{vt(p-p_j-q)}{\hbar}\right] \bar{\rho}_d(p-q)
\end{aligned} \tag{6}$$

$$\begin{aligned}
& \partial_t \bar{\rho}_d(p) \\
&= \frac{2t}{\hbar^2} \int_{-\infty}^{\infty} dq \tilde{G}_0(q) \text{sinc}\left[\frac{vtq}{\hbar}\right] \{ \bar{\rho}_d(p-q) - \bar{\rho}_d(p) \} \\
&\quad - \sum_{j=1,2} \frac{tC_0(1-\delta_{ab})}{\hbar^2} \text{sinc}\left[\frac{vt(p-p_j)}{\hbar}\right] \bar{\rho}_d(p) \\
&\quad + \sum_{j=1,2} \frac{4t}{\hbar^2} \text{sinc}\left[\frac{vt(p-p_j)}{\hbar}\right] \int_{-\infty}^{\infty} dq \tilde{G}_1(q) \bar{\rho}_f(p-q)
\end{aligned} \tag{7}$$

Assume the dispersive band state component is negligible with $\bar{\rho}_d = 0$ since we focus on the short time evolution of initial flat-band state, the time-nonlocal master equation for the flat-band Eq. (6) is simplified into:

$$\begin{aligned}
\partial_t \bar{\rho}_f(p) &= - \sum_{j=1,2} \Gamma_t^{(j)}(p-p_j) \bar{\rho}_f(p) \\
&\quad + \frac{t(1+\delta_{ab})}{\hbar^2} \int_{-\infty}^{\infty} dq G_0(q) \left[\bar{\rho}_f(p-q) - \bar{\rho}_f(p) \right]
\end{aligned} \tag{8}$$

where $\Gamma_t(p) = \frac{1-\delta_{ab}}{\hbar^2} \int_{-\infty}^{\infty} dq G_0(q) t \text{sinc}\left[\frac{vt(q-p)}{\hbar}\right]$. The first term in Eq. (8) describes the decay process, while the second term describes the dephasing process. Note that $\text{sinc}\left[\frac{vt(q-p)}{\hbar}\right] = \int_{-1/2}^{1/2} dx \exp\left[\frac{2ivt(q-p)x}{\hbar}\right]$, after some algebra we obtained

$$\begin{aligned}
\Gamma_t(p) &= \frac{1-\delta_{ab}}{2\hbar} \frac{\pi i}{v} G_0(p) \\
&\quad \times \left[\text{Erfi}\left[\frac{p\ell}{2\hbar} - \frac{itv}{\ell}\right] - \text{Erfi}\left[\frac{p\ell}{2\hbar} + \frac{itv}{\ell}\right] \right]
\end{aligned} \tag{9}$$

where Erfi is the imaginary error function.

The detailed derivation of master equations for both the flat and dispersive band is provided in supplementary materials [30].

Numerical results.—In order to estimate the validity of the disorder master equations Eq. (8), we numerically diagonalize the 1D-cross-stitch model under the periodic boundary condition with $N = 100$ unit cells, and average over $K = 200$ disorder realizations. A Gaussian wave packet initially on the flat band is con-

sidered, $\psi_0(x) = \frac{1}{\sqrt{\sqrt{\pi}\sigma}} \exp\{- (x-x_0)^2/(2\xi^2) + ip_0x\}$, centered around $x_0 = 50a$ with position uncertainty $\xi^2 = 12a^2$, p_0 is the initial average momentum. The subsequent time evolution is performed by obtaining all energy eigenvalues ε_n and the corresponding eigenvectors ψ_n of the full Hamiltonian \hat{H}_ε and then evaluating $|\psi(t)\rangle = \sum_n \exp\{-i\varepsilon_n t\} \langle \psi_n | \psi_0 \rangle | \psi_n \rangle$.

For a fixed intra-cell hopping value $t_{ab} = 1.0$, the two intersections are $p_{1,2} = \pm 2.09 \hbar/a$ and the velocities are $v_{1,2} = \pm 3.46 aJ/\hbar$. We perform the time evolution in two cases: (i) the initial state partially overlaps with one of the intersections such as p_1 , i.e. the resonant case with $p_0 = 1.26 \hbar/a$ or (ii) $p_0 = 0$, the detuned case. The decay of initial flat-band state into the dis-

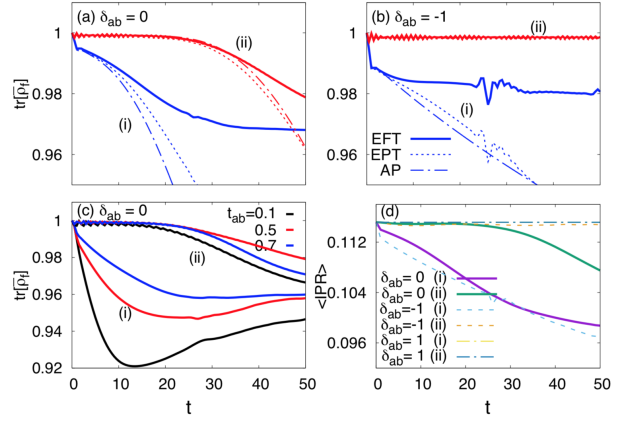


FIG. 2. (Color online) Comparison of exact full trace (EFT) and analytic prediction (AP) Eq. (8) for disorder-induced wave-packet dynamics. The initial state is on the flat-band, (i) in resonant with or (ii) detuned from the intersections, in (a),(b). In (a), steady decay (i) or delayed decay (ii) into dispersive band are found. Tuning disorder correlations $\delta_{ab} = -1$ we find contrasting dynamics in (b). Exact partial trace (EPT) agrees better with AP. (c) Tune the location of the flat-band, interference effect between the two intersections is observed for $t_{ab} = 0.5, 0.7$. (d) The ensemble average $\langle \text{IPR} \rangle$ of flat-band for different cases.

pulsive band varies, determined by p_0 , the velocity v at the intersection and the disorder correlations. In the limit of no correlations with $C_{aa}(x) = C_{bb}(x) = C_0\delta(x)$, the wave-packet collapses immediately. For $\delta_{ab} = 0$ we have $G_1(q) = 0$, i.e., Gaussian correlation is set in each sublattice while no correlations between a and b sublattices. Fig. 2(a) display the disorder-induced flat-band state decay obtained from ED calculations or the analytic predictions Eq. (8), respectively. The steady decay into dispersive band starts at the beginning in (i) due to the partial overlap with intersection p_1 while the detuned initial state in (ii) has a delayed decay. This delayed decay is limited by the intra-channel dephasing-mediated momentum diffusion [29]. Intra-channel dephasing vanishes in Eq. (8) when $\delta_{ab} = -1$ and the delayed decay is absent in (b)(ii). Note that, the $\delta_{ab} = 1$ case in

(c) describes perfectly correlated sub-lattice potentials with $V_\varepsilon^a(j) = V_\varepsilon^b(j)$ in which case the flat and dispersive band are decoupled completely. The momentum distribution broadening term, i.e. the second term in RHS of Eq. (8), preserves the trace of flat component as the initial value. In our numerical experiments, we track the trace of flat-band state partially in the range $[x_0 - 8a, x_0 + 8a]$ in real space in comparison with the full trace. The former agrees better with analytical predictions. Because the dispersive component partly reenters the flat-band, leading to a diffusive delocalization on the flat-band. In (c), for the resonant case (i) where the wave packet is close to one of the intersection, the dynamics changes monotonically as t_{ab} varies. However for (ii) where the wave packet is in the middle of the two intersections, we observe interference pattern as the distance of two intersections changes, e.g. $t_{ab} = 0.5, 0.7$. In (d), we analyze the inverse participation ratio (IPR) to quantify the distribution of flat-band wave packet, where $\text{IPR}(t) = \sum_j I_j^2(t) / \sum_j I_j(t)$ and the total intensity in each unit cell is defined as $I_j(t) = |a_j(t)|^2 + |b_j(t)|^2$. Consistent with the previous result, the trivial decoupled $\delta_{ab} = 1$ case shows no diffusion. For $\delta_{ab} = 0$ or -1 , the detuned case (ii) have significantly modified diffusion magnitudes compared to (i) case. Symmetric and non-symmetric diffusions could be found in the distribution of $I_j(t)$ [30].

2D model.— The $\alpha - T_3$ model is a triangular Bravais lattice with three sites A, B, C per unit cell, as shown in Fig. 3 (a). The hopping amplitude between sites A and B is $C_\alpha J = \frac{J}{\sqrt{1+\alpha^2}}$, while between sites B and C it is $S_\alpha J = \frac{\alpha J}{\sqrt{1+\alpha^2}}$. Note that the hopping between A and C is not permitted. In continuum limit with no on-site potential, one flat-band with energy $E_0 = 0$ and two dispersive bands E_\pm are presented regardless of α [30]. Interestingly, tuning α from 0 to 1 could continuously change the Berry phase. In site basis $\Psi_{m,n} = (\Psi_{m,n}^A, \Psi_{m,n}^B, \Psi_{m,n}^C)^T$ with armchair edges in the x direction and periodic boundary condition in y , the nanotube tight-binding model is ($J = 1$ for simplicity) [33, 34]:

$$\begin{aligned}
-C_\alpha \Psi_{m,n}^B - C_\alpha \Psi_{m-1,n-1}^B - C_\alpha \Psi_{m+1,n}^B &= E \Psi_{m,n}^A, \\
-C_\alpha \Psi_{m,n}^A - C_\alpha \Psi_{m-1,n}^A - C_\alpha \Psi_{m+1,n+1}^A &= E \Psi_{m,n}^B, \\
-S_\alpha \Psi_{m,n}^C - S_\alpha \Psi_{m-1,n-1}^C - S_\alpha \Psi_{m+1,n}^C &= E \Psi_{m,n}^B, \\
-S_\alpha \Psi_{m,n}^B - S_\alpha \Psi_{m-1,n}^B - S_\alpha \Psi_{m+1,n+1}^B &= E \Psi_{m,n}^C.
\end{aligned} \tag{10}$$

Fig. 3 (b) gives the band structure of $\alpha - T_3$ armchair nanotube which displays the 0 energy flat-band states and band crossings at $k_y = 0$. Explicitly, central B site does not reveal the presence of the flat-band but only A or C sites have contributions. For $\alpha - T_3$ nanotube with finite size $N_x \times N_y$, we initial a flat-band

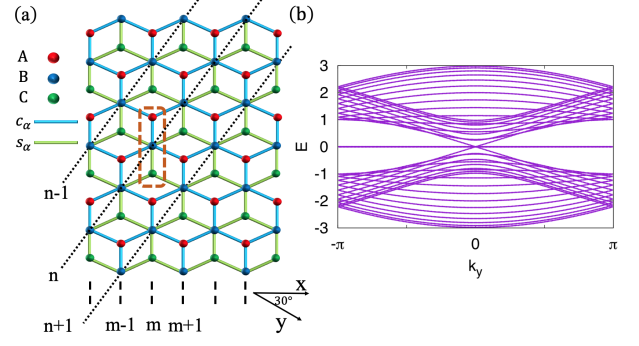


FIG. 3. (Color online) (a) An armchair nanotube structure from $\alpha - T_3$ lattice. Only nearest-neighbor hoppings are considered. Blue links represent hoppings between A and B sites with amplitude $C_\alpha = \frac{1}{\sqrt{1+\alpha^2}}$ (in unit of J), and green links are hoppings between B and C atoms with amplitude $S_\alpha = \frac{\alpha}{\sqrt{1+\alpha^2}}$ such that $C_\alpha^2 + S_\alpha^2 = 1$. The location of unit cell is labelled by m, n in the real space. (b) Band structure of armchair nanotube with width $N_x = 20$. Note that the spectrum does not depend on α .

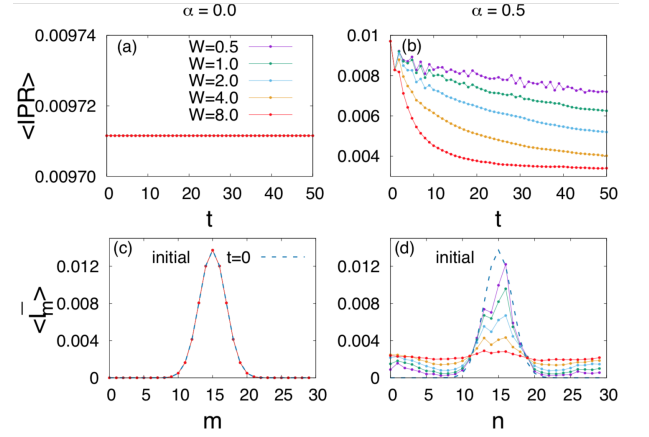


FIG. 4. (Color online) (a-b) The ensemble average $\langle \text{IPR} \rangle$ versus time t . Time evolution is involved in $N_x \times N_y$ armchair nanotube system with $N_x = 30, N_y = 15$, averaging over $K = 100$ disorder realizations. Disorder strength W ranges from 0.5 – 8.0. (c-d) Disorder averaged mean intensity profile $\langle I_m \rangle$ at $t = 50$. Dashed line represents the initial mean intensity profile. The left and right columns corresponds to $\alpha = 0, 0.5$.

state with a Gaussian prefactor in x direction $\psi_{f,0} \sim \exp \left[-\frac{(x-x_0)^2}{2\xi^2} + ip_{0x}x \right] \Psi_f$ where $\Psi_f = (S_\alpha, 0, -C_\alpha)^T$, $x_0 = N_x/2$. In spite of intersections between flat and dispersive bands, the dynamics of such a wave packet remains unchanged in the absence of disorders. Here we focus on the dynamics of the isolated compact flat-band mode in the presence of correlated disorders $V_\varepsilon^\sigma(\vec{r})$ on the lattice with only intra-sublattice correlation $C_{\sigma\sigma}(\vec{r}) = C_0 e^{-(|r-r'|^2/l^2)}$ where $\sigma \in \{A, B, C\}$.

In Fig. 4(a)(b) we illustrate the dynamics of the disorder-

der average $\langle \text{IPR} \rangle$ and quantify the dependence on different disorder strength W . When $\alpha = 0$, flat-band states $\psi_{f,0}$ are trapped in isolated sites C in the middle honeycomb lattice with no hoppings to the other sites.

The numerically calculated IPR confirm the presence of localization in (a). In contrast, flat-band states are set up in A and C sites initially when $\alpha \neq 0$. Correlated disorder brings inverse Anderson localization to the flat-band mode. Significantly more number of sites are populated under stronger disorder strength W . Note that larger α could also enhance the rate of diffusion gradually. Since the initial wave packets are uniformly distributed in y direction, we display the mean intensity $\bar{I}_m = \sum_n I_{mn}/N_y$ as a function of the lattice index m in x direction after a propagation of $t = 50$. Intuitively, the $\alpha = 0$ case preserves its initial intensity profile while Fig. 4(d) shows the breakdown of compact localization in $\alpha - T_3$. Stronger disorders induce wider spreading but transitions to regular Anderson localization are not observed.

Conclusion.—We investigate the wave-packet dynamics in presence of correlated disorders with the band-structure of flat-bands intersecting with dispersive bands, in 1D and 2D. In 1D cross-stitch model, we find the momentum-dependent decay of flat-band states is delayed when the initial flat-band state is detuned from the intersection. With the help of time-resolved quantum master equation, we show the dephasing-mediated decay limiting the delay through momentum broadening.

In 2D $\alpha - T_3$ model, we construct nanotube structure with armchair edges in finite size and numerically investigate the spreading of flat-band state wave packet. Predictably, flat-band states are trapped in C sites when $\alpha = 0$ in spite of the presence of disorders and intersections. The situations are totally different when $\alpha \neq 0$ where inverse Anderson localization is observed in the presence the correlated disorders. The rate and extent of diffusion could be enhanced with stronger disorder strength or larger α . Due to the complexity in 2D with much more bands, analytic expression using master equations is absent here. Nevertheless, we believe all our predictions here can be checked in future theoretical and experiment work.

ACKNOWLEDGMENTS

The authors thank Clemens Gneiting for helpful discussions. The work is supported by NSFC Grant No. 61988102, the Key Research and Development Program of Guangdong Province (2019B090917007) and the Science and Technology Planning Project of Guangdong Province (2019B090909011). Z. L. acknowledges the support of funding from Chinese Academy of Science E1Z1D10200 and E2Z2D10200; from ZJ project 2021QN02X159 and from JSPS Grant No. PE14052 and P16027. Z.-X. H. was supported by NSFC Grant

No. 11974064, No.12147102, and the Fundamental Research Funds for the Central Universities under Grant No. 2020CDJQY-Z003.

* liz@aircas.ac.cn

- [1] E. H. Lieb, *Phys. Rev. Lett.* **62**, 1201 (1989).
- [2] Z. Gulácsi, A. Kampf and D. Vollhardt, *Phys. Rev. Lett.* **99**, 026404 (2007).
- [3] H. Tasaki, *Phys. Rev. Lett.* **69**, 1608 (1992).
- [4] A. Mielke and H. Tasaki, *Comm. Math. Phys.* **158**, 341 (1993).
- [5] M. Johansson, U. Naether, and R. A. Vicencio, *Phys. Rev. E* **92**, 032912 (2015).
- [6] Z. Li, D. Baillie, C. Blois, and F. Marsiglio, *Phys. Rev. B* **81**, 115114 (2010).
- [7] K. Sun, Z.-C. Gu, H. Katsura, and S. Das Sarma, *Phys. Rev. Lett.* **106**, 236803 (2011).
- [8] Y.-F. Wang, Z.-C. Gu, C.-D. Gong, and D. N. Sheng, *Phys. Rev. Lett.* **107**, 146803 (2011).
- [9] F. Wang and Y. Ran, *Phys. Rev. B* **84**, 241103(R) (2011).
- [10] J. D. Malcolm and E. J. Nicol, *Phys. Rev. B* **92**, 035118 (2015).
- [11] E. Illes, J. P. Carbotte, and E. J. Nicol, *Phys. Rev. B* **92**, 245410 (2015).
- [12] Z. Li and J. P. Carbotte, *Phys. Rev. B* **89**, 085413 (2014).
- [13] L. D. Xian, D. M. Kennes, N. T. Dejean, M. Altarelli, and A. Rubio, *Nano Lett.* **2019**, *19*, *8*, 4934–4940
- [14] Q. Li, B. Cheng, M. Y. Chen, B. Xie, Y. Q. Xie, P. F. Wang, F. Q. Chen, Z. L. Liu, K. Watanabe, T. Taniguchi, S.-J. Liang, D. Wang, C. J. Wang, Q.-H. Wang, J. P. Liu and F. Miao, *Nature* **609**, pages479–484 (2022)
- [15] S. d. Tao, X. L. Zhang, J. J. Zhu, P. M. He, S. Y. A. Yang, Y. H. Lu and S.-H. Wei, *Journal of the American Chemical Society* **2022**, *144* (9), 3949-3956.
- [16] M. C. Rechtsman, J. M. Zeuner, Y. Plotnik, Y. Lumer, D. Podolsky, F. Dreisow, S. Nolte, M. Segev, and A. Szameit, *Nature* **496**, 196 (2013).
- [17] F. D. M. Haldane and S. Raghu, *Phys. Rev. Lett.* **100**, 013904 (2008).
- [18] N. Y. Kim, K. Kusudo, C. Wu, N. Masumoto, A. Löffler, S. Höfling, N. Kumada, L. Worschech, A. Forchel, and Y. Yamamoto, *Nature Phys* **7**, 681 (2011).
- [19] R. A. Vicencio, C. Cantillano, L. Morales-Inostroza, B. Real, C. Mejía-Cortés, S. Weimann, A. Szameit, and M. I. Molina, *Phys. Rev. Lett.* **114**, 245503 (2015).
- [20] S. Mukherjee, A. Spracklen, D. Choudhury, N. Goldman, P. Öhberg, E. Andersson, and R. R. Thomson, *Phys. Rev. Lett.* **114**, 245504 (2015).
- [21] G. Gligorić, D. Leykam, and A. Maluckov, *Phys. Rev. A* **101**, 023839 (2020).
- [22] S. Longhi, *Opt. Lett.* **46**, 2872 (2021).
- [23] M. Kremer, I. Petrides, E. Meyer, M. Heinrich, O. Zilberberg, and A. Szameit, *Nat. Commun.* **11**, 907 (2020).
- [24] S. Mukherjee, M. D. Liberto, P. Öhberg, R. R. Thomson, and N. Goldman, *Phys. Rev. Lett.* **121**, 075502 (2018).
- [25] H. Li, Z. L. Dong, S. Longhi, Q. Liang, D. Z. Xie, and B. Yan, *Phys. Rev. Lett.* **129**, 220403 (2022).
- [26] F. M. Izrailev, A. A. Krokhnin, N. M. Makarov, *Phys. Rep.* **512**, 125 (2012).
- [27] C. Gneiting and F. Nori, *Phys. Rev. A* **96**, 022135 (2017).

- [28] C. Gneiting and F. Nori, *Phys. Rev. Lett.* **119**, 176802 (2017).
- [29] C. Gneiting, Z. Li and F. Nori, *Phys. Rev. B* **98**, 134203 (2018).
- [30] See Supplemental Material at <http://.....> for a detailed derivations and more numerical results.
- [31] J. D. Bodyfelt, D. Leykam, C. Danieli, X. Yu, and S. Flach, *Phys. Rev. Lett.* **113**, 236403 (2014).
- [32] S. Flach, D. Leykam, J. D. Bodyfelt, P. Matthies, and A. S. Desyatnikov, *Europhys. Lett.* **105**, 30001 (2014).
- [33] M. Kohmoto and Y. Hasegawa, *Phys. Rev. B* **76**, 205402 (2007).
- [34] Y. R. Chen, Y. Xu, J. Wang, J. F. Liu, and Z. S. Ma, *Phys. Rev. B* **99**, 045420 (2019).